Materials Horizons

COMMUNICATION

View Article Online
View Journal | View Issue

Cite this: *Mater. Horiz.*, 2020, 7, 223

Received 19th March 2019,
Accepted 23rd August 2019

DOI: 10.1039/c9mh00409b

rsc.li/materials-horizons

Locking of phase transition in MOF ZIF-7: improved selectivity in mixed-matrix membranes for O_2/N_2 separation†

Long Xiang,‡[a] Donghui Liu,‡[a] Hua Jin,‡[b] Long-Wei Xu,[a] Chongqing Wang,[a] Shutao Xu,*[c] Yichang Pan*[a] and Yanshuo Li*[b]

The framework flexibility of metal–organic frameworks (MOFs) is beneficial for gas storage and adsorption but is disadvantageous to the separation process based on the size-extrusion mechanism. Herein, the framework flexibility of ZIF-7, a typical MOF famous for its phase transition between wide-pore (ZIF-7-I) and narrow-pore (ZIF-7-II) forms on desolvation, was successfully hindered by embedding MOF nanocrystals in the rigid polymer matrix. For the first time, it was experimentally demonstrated that ZIF-7 could be "locked" in the wide-pore phase (ZIF-7-I) even after complete desolvation. A mixed-matrix membrane containing ZIF-7-I nanocrystals and rigid polyimides showed O_2 permeability of 3 Barrer and O_2/N_2 selectivity of 15, surpassing the state-of-the-art upper limit for O_2/N_2 and falling in the commercially attractive region. In view of the weak competitive interaction between O_2/N_2 and hybrid membrane materials, similar permeation results were also found for the separation of equal-molar O_2/N_2 binary mixtures.

New concepts

The phase transition of metal–organic frameworks (MOFs) is usually accompanied by their porous structure changes. This is the origin of the framework flexibility, one of the most interesting characteristics of MOFs. However, it also exhibits obvious disadvantages while MOF adsorbents distinguish different guest species based on the size exclusion mechanism. Unlike the reported complex methods for controlling the framework flexibility of MOFs through fine-adjusting the composition, morphology and guest-occupation of MOFs, a new concept was demonstrated in this work, namely, locking of the phase transition by embedding the MOF nanocrystals in the rigid polymer matrix to control its framework flexibility. As exemplified by highly flexible MOF ZIF-7, its phase transition derived from desolvation could be effectively hindered by embedding in a rigid polyimide matrix. The resulting composite membranes showed an air separation performance surpassing the state-of-the-art upper limit and falling in the commercially attractive region. It is believable that the proposed strategy is also suitable for controlling the framework flexibility of other MOFs. This approach will facilitate the application of MOFs as rigid "molecular-sieve" materials in adsorption and separation membranes.

Oxygen separation from air is important for many industrial processes such as medical treatments, steel production and oxy-fuel combustion. Currently, air separation is achieved primarily by energy-intensive cryogenic distillation and pressure swing adsorption (PSA).[1–3] Oxygen selective membranes can provide a more energy-efficient alternative to cryogenic separation and PSA process. The pore size of zeolite 4A falls between the molecular sizes of O_2 and N_2 (O_2: 3.8 Å × 2.8 Å, N_2: 4.2 Å × 3.2 Å) and thus, it is presumably considered as an ideal membrane material for O_2/N_2 separation. However, the O_2/N_2 separation factor of the zeolite 4A membranes obtained so far is still below 10.[4] This is because although the N_2 molecule is more bulky than the O_2 molecule, due to its larger quadrupole moment, it interacts more strongly with the extra-framework cations of zeolites than O_2. In this regard, a neutral framework with a smaller pore size (<0.4 nm) is more ideal. The zeolitic imidazolate framework-7 ($Zn(benzimidazole)_2$, ZIF-7), a typical metal–organic framework (MOF), is one such candidate.[5] It has sodalite topology with a crystallographic pore size of 3.0 Å. Molecular sieving separation of O_2 and N_2 is therefore expected.

Framework flexibility is one the most interesting characteristics of MOFs and is different to that of the porous network compounds based on purely inorganic building units.[6–8] By the virtue of its flexible advantages, MOFs used as storage agents or adsorbents are very useful for practical applications due to the enlargement of the uptake difference between the charge and discharge pressures.[9,10] However, it also exhibits obvious disadvantages while MOF adsorbents distinguish different guest species based on the size exclusion mechanism. For example, as one of the hot individuals, the zeolitic imidazolate framework ZIF-8, whose

[a] *College of Chemical Engineering, State Key Laboratory of Materials-Oriented Chemical Engineering, Nanjing Tech University, Nanjing 210009, P. R. China. E-mail: panyc@njtech.edu.cn*
[b] *The School of Materials Science and Chemical Engineering, Ningbo University, Ningbo 315211, P. R. China. E-mail: liyanshuo@nbu.edu.cn*
[c] *National Engineering Laboratory for Methanol to Olefins, Dalian National Laboratory for Clean Energy, iChEM, Dalian Institute of Chemical Physics, Chinese Academy of Sciences, Dalian 116023, China. E-mail: xushutao@dicp.ac.cn*

† Electronic supplementary information (ESI) available. See DOI: 10.1039/c9mh00409b

‡ These authors contributed equally to this work.

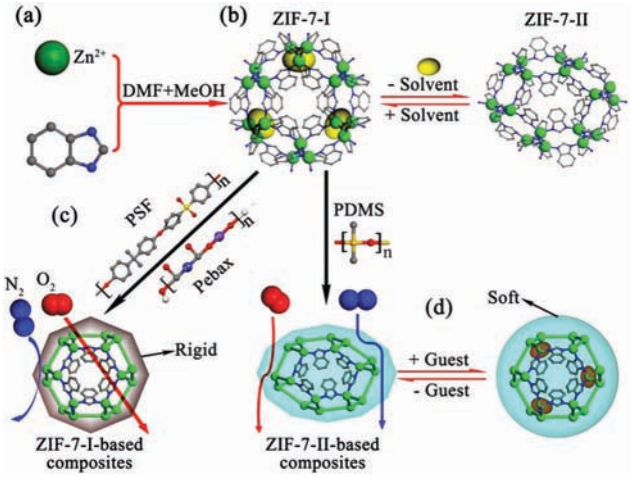

Scheme 1 Illustration of fabricating ZIF-7-polymer composites in this study. (a) ZIF-7 synthesized from zinc ions and benzimidazoles; (b) phase transitions in ZIF-7 framework; (c) combination of polymer matrix with different rigidities (PSF, Pebax®1657 or PDMS) and ZIF-7 nanoparticles to form mixed-matrix membranes for O_2/N_2 separation; (d) reversible breathing behavior of ZIF-7-II-polymer composites.

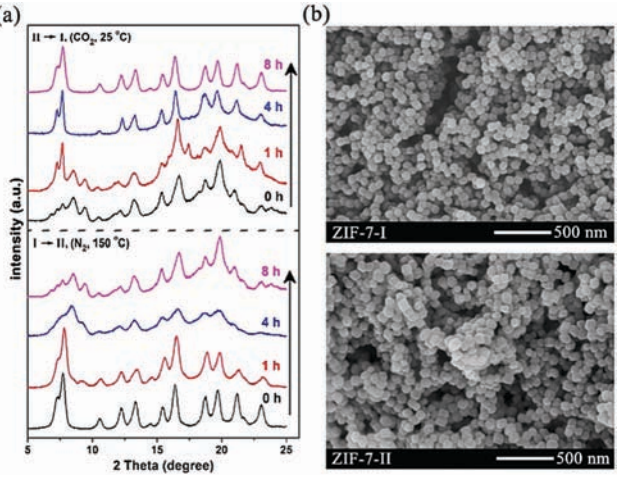

Fig. 1 (a) XRD patterns and (b) SEM images of as-synthesized ZIF-7-I and ZIF-7-II nanocrystals. The phase transition from ZIF-7-I to ZIF-7-II structure was conducted at 150 °C with the purge of N_2, while phase transition from ZIF-7-II to ZIF-7-I was performed at 25 °C with the purge of pure CO_2.

crystallographic pore size (~3.4 Å) falls between the critical diameters of CO_2 (~3.3 Å) and CH_4 (~3.8 Å),[5,11] is expected as an ideal candidate for CO_2/CH_4 separation by molecular sieving. However, the well-intergrown ZIF-8 polycrystalline membrane does not exhibit an effective performance for CO_2/CH_4 separation. Fortunately, extensive research has demonstrated that its effective aperture is 4.0–4.2 Å, which is just between the kinetic diameters of C_3H_6 (4.0 Å) and C_3H_8 (4.2 Å).[12] As a result, the ZIF-8 polycrystalline membrane exhibits an impressive separation performance for C_3H_6/C_3H_8 separation.[13–17] ZIF-7 is famous for its phase transition between wide-pore (ZIF-7-I) and narrow-pore (ZIF-7-II) forms on desolvation[18,19] (Scheme 1). Therefore, an ideal ZIF-7 membrane should be made of the ZIF-7-I phase. This means that the flexibility of ZIF-7 should be effectively hindered during desolvation activation. Herein, we developed a facile strategy for hindering the flexibility of MOFs by embedding in rigid polymers. It was convenient to detect the flexibility behavior, *i.e.*, phase transition by physical characterizations. The phenomenon of hindering the ZIF-7 flexibility in the polymer was strongly dependent on the intrinsic rigidity of the polymer matrix (Scheme 1c). A glassy polymer with a high T_g value could effectively hinder the phase transition of ZIF-7, and the resulting mixed-matrix membranes (MMMs) exhibited an impressive performance for O_2/N_2 separation, surpassing the Robeson upper limit reported in 2008.[20]

ZIF-7 nanocrystals were first synthesized based on our previously reported methods.[21] *In situ* X-ray diffraction (XRD) measurements indicated that the complete removal of the occupied solvents, namely, dimethylformamide (DMF) and methanol (MeOH) in the as-synthesized ZIF-7 nanocrystals could lead to a phase transition from ZIF-7-I to ZIF-7-II (Fig. 1a). We also found that this phase transition could be reversible (*i.e.*, ZIF-7-II to ZIF-7-I) when the ZIF-7-II nanocrystals were either purged with a pure CO_2 gas or immersed in several kinds of solvents and not just in DMF, as reported by Redfern and co-workers[18] (Fig. 1a and Fig. S2 in the ESI†). This result indicated that the two ZIF-7 phase structures are inter-changeable due to the gain and loss of the occupied guests, verifying the intrinsic flexibility of the ZIF-7 framework. The XRD peak broadening was due to the nanosized crystals. Scanning electron microscopy (SEM) images (Fig. 1b) also showed that the phase transition process did not alter both the particle size (80–100 nm) and morphology (hexahedral-cubic shape) of these two kinds of ZIF-7 nanocrystals.

Since the glass transition temperature (T_g) determined by the differential scanning calorimetry (DSC) technique can provide qualitative estimation of the rigidity of polymers,[22] three commercial polymers with different rigidities were used as the matrices to embed the ZIF-7 nanocrystals for evaluating the hindered phase transition. The T_g values for PDMS, Pebax®1657 and PSF were −120, −56 and 187 °C, respectively. The as-synthesized ZIF-7-polymer composites were vacuum-dried at 150 °C for a week. To prove that there was no residual solvent in the ZIF-7-polymer composites, solid state ^{13}C NMR and thermogravimetric mass spectrometry (TG-MS) were first conducted. Correspondingly, the ^{13}C NMR peaks of chloroform ($\delta \sim 77$ ppm), ethanol ($\delta \sim 17.4$, 57.9 ppm) and *n*-heptane ($\delta \sim 14.1$, 22.7, 29, 31.8 ppm) did not appear for the corresponding MMMs fabricated from PSF, Pebax®1657 and PDMS. As shown in Fig. 2b and Fig. S3 (ESI†), no ion current peaks of $m/z = 119$ ($CHCl_3$), 46 (C_2H_5OH) and 100 (C_7H_{16}) are observed during the whole process of pyrolysis for the above three composites. In addition, TGA plots also showed that the weights of the hybrid samples remained constant between 50 °C and 150 °C, indicating that there were no water molecules in the composites. Therefore, these results strongly suggest that all the solvents in the ZIF-7-polymer composites have been completely removed. XRD patterns indicated that the phase structure of the ZIF-7 nanocrystals was strongly dependent on the polymer matrix (Fig. 2c). The ZIF-7 nanocrystals exhibited a type-II structure in the PDMS matrix but a type-I structure was observed in the PSF and Pebax®1657 matrices. This result was consistent with the disparity

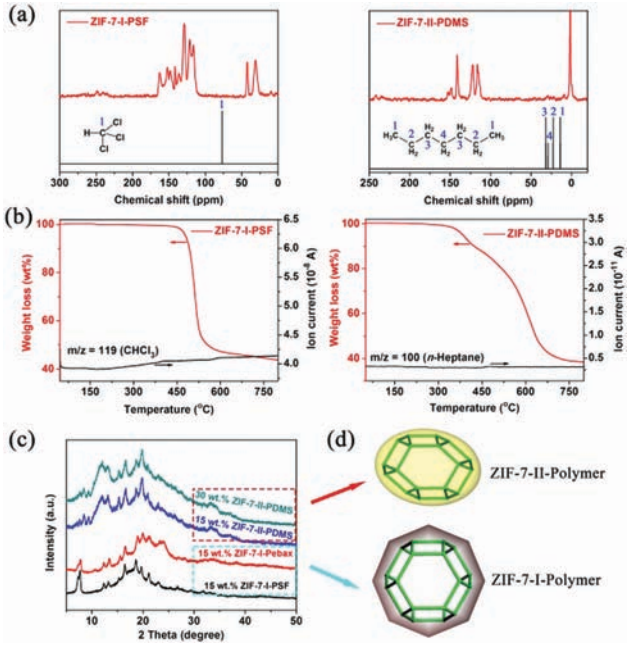

Fig. 2 (a) Solid-state ^{13}C CP-MAS NMR spectra, (b) TGA and ion current trace curves, (c) XRD patterns and (d) structural schematic diagram of ZIF-7-polymer composites derived from three commercial polymers.

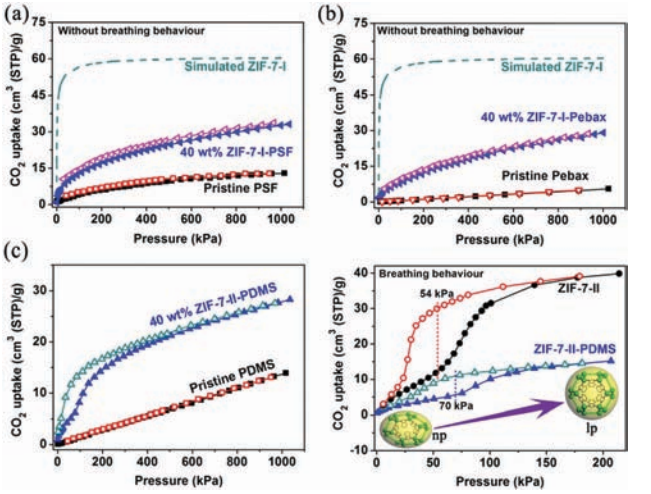

Fig. 3 CO_2 adsorption properties of pristine polymer, ZIF-7 nanocrystals and 40 wt% ZIF-7-polymer composites derived from (a) PSF, (b) Pebax®1657 and (c) PDMS. Closed and open symbols represent adsorption and desorption branches, respectively. The dashed line is the GCMC adsorption of the ZIF-7-I phase. ZIF-7-II-PDMS composite can be reversibly transformed from a narrow pore (type-II) to a large pore (type-I) phase. The CO_2 uptake for all samples was assessed in the high-pressure region (up to 10 bar) by analysis of the respective isotherms measured at 308 K.

of the polymer chain mobility (PDMS > Pebax®1657 > PSF), suggesting that flexible PDMS could not effectively hinder the phase transition of ZIF-7 (Fig. 2d).

For the highly flexible ZIF-7 framework, a CO_2-induced "breathing" performance[23] is another route to evaluate its phase transition phenomenon. As shown in Fig. 3a, the pristine PSF polymer and 40 wt% ZIF-7-I-PSF composite exhibit a typical dual-mode sorption curve of a glassy polymer. As a rubbery polymer, the CO_2 adsorption on Pebax®1657 exhibits a Henry behaviour, showing a linear isotherm (Fig. 3b). However, the CO_2 isotherm for the 40 wt% ZIF-7-I-Pebax®1657 composite was more Langmuirian. This phenomenon was due to the improved CO_2 adsorption from the blended ZIF-7-I nanocrystals. Since the ZIF-7-I structure was occupied by solvents, its porosity and adsorptive property could not be determined by experimental sorption measurements. Therefore, the CO_2 adsorption isotherms for the ZIF-7-I crystals were obtained through Grand Canonical Monte Carlo (GCMC) simulations.[24] It was found that the isotherm exhibited a general trend of monotonic and smooth increase (Fig. 3a and b). Therefore, a reversible CO_2 adsorption/desorption behaviour (without hysteresis) on both the PSF- and Pebax®1657-based composites implied that the ZIF-7 framework invariably contained a large-pore phase (type-I structure) in PSF and Pebax®1657 matrices and was thus without the "breathing" behavior for CO_2 sorption. In contrast, the CO_2 adsorption isotherms of the ZIF-7-II-PDMS composite showed quite opposite results, presenting a step change during CO_2 uptake with hysteresis (Fig. 3c). This corresponded to a common feature of flexible frameworks, which was similar to the breathing behavior of the ZIF-7-II crystals.[25–27] However, the gate-opening pressure (~70 kPa) for the 40 wt% ZIF-7-II-PDMS composite was higher than that of pure ZIF-7-II crystals (~54 kPa). Even on the PDMS-based MMMs containing 15 wt% fillers, the reversible transformation from narrow-pore ZIF-7-II to wide-pore ZIF-7-I occurred (Fig. S4 in the ESI†). The above results suggested that the PDMS polymer ought to reduce the flexibility of the ZIF-7 framework. Based on above results, it is clear that the phase transition of the ZIF-7 framework in composites is dependent on the rigidity of the polymer. In general, the chain flexibility of polymers is determined by two factors. One is the character of the main chain, and the other is the presence and nature of the side chains or side groups. For the bisphenol A-derived PSF, highly conjugated aromatic ring systems derived from both the phenylene and diphenylsulfone groups make the main chain very rigid and difficult to rotate. Pebax®1657, a thermoplastic poly-(ether-*block*-amide) polymer, consists of linear chains of rigid polyamide (PA) blocks covalently linked to soft polyether (PE) blocks *via* ester groups. The PA segments provide rigidity for hindering the phase transition of ZIF-7. On the contrary, PDMS comprises a sequence of –Si–O– units. The rotation energy of this inorganic polymer is very low and thus, it is highly flexible.

By virtue of the hindered phase transition, the ZIF-7-I nanocrystals blended in the PSF matrix were considered as ideal fillers for O_2/N_2 separation due to their suitable crystallographic pore size (~3.0 Å). Furthermore, the combination of the attractive properties of polymeric and MOF materials to form mixed-matrix membranes (MMMs) is considered as a facile strategy for overcoming the trade-off between gas permeability and selectivity for a pristine polymer membrane.[28] As shown in Fig. 4a, the fabricated MMMs are warped and return to their initial shape without any flaws due to the intrinsic

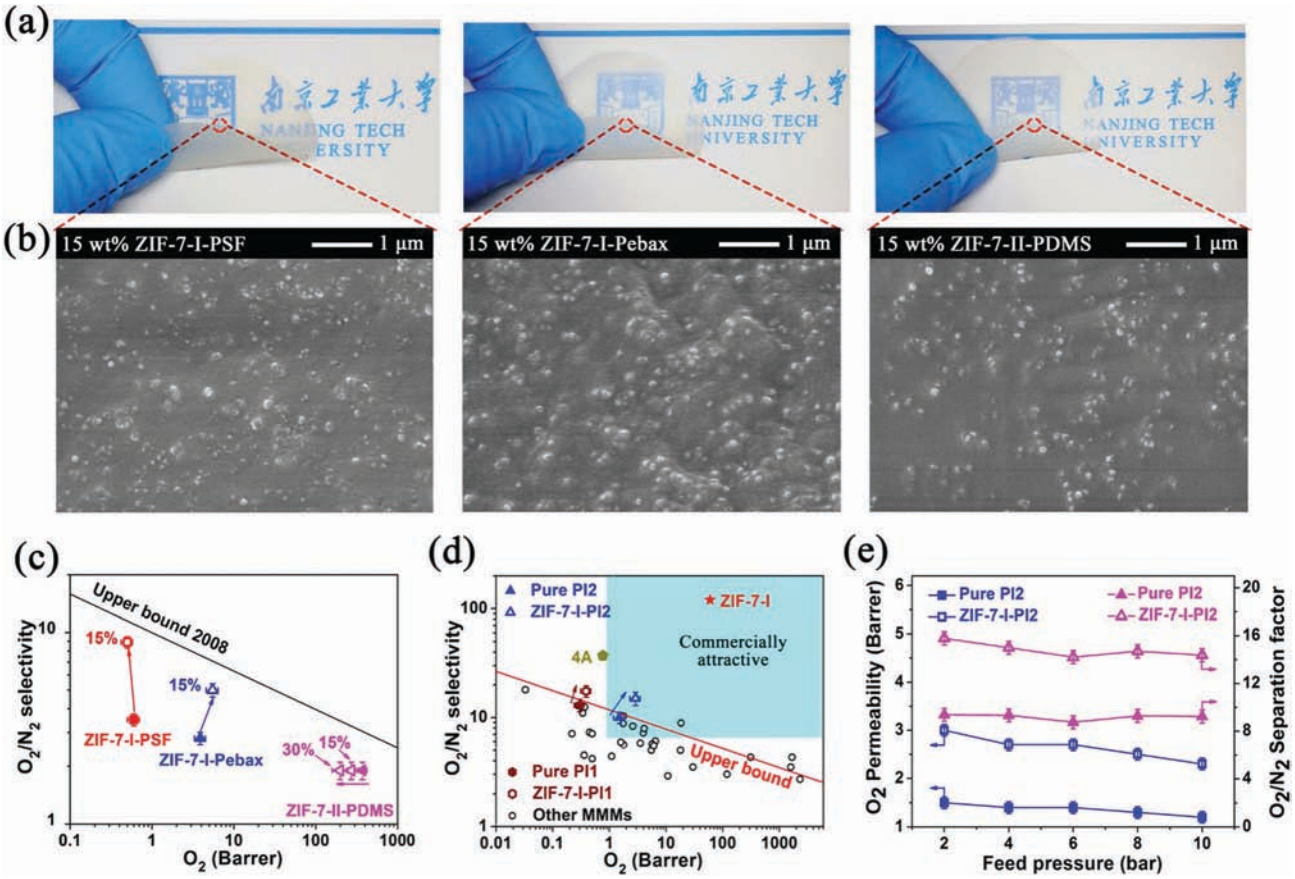

Fig. 4 (a) The physical appearance, (b) SEM images of cross-sections, (c) pure component O_2 and N_2 permeation properties measured at 2 bar upstream pressure and 35 °C, and (d) comparison of O_2/N_2 separation performance in this work with the other MMMs. The commercially attractive region was identified by Koros and co-workers;[32] (e) O_2/N_2 (50 : 50) mixed-gas permeation results as a function of feed pressure on the pristine 6FDA/BPDA-ODA (PI2) films and 15 wt% ZIF-7-I-PI2 membranes. The total feed pressure and permeating temperature are 4 bar and 35 °C, respectively. Closed and open symbols represent the results of pristine PI2 film and 15% ZIF-7-I-PI2 membranes, respectively.

mechanical strength of the polymer matrices. All membranes were transparent with the thickness of 60 ± 20 μm (Fig. S5, ESI†). After the combination of optimized dispersing and casting conditions, the ZIF-7 fillers were uniformly distributed in the polymer matrices (Fig. 4b). This positive morphology strongly confirmed that the fabricated MMMs were defect-free. Otherwise, obvious signs of microscale phase segregation or aggregates were observed on the as-synthesized MMMs (Fig. S6, ESI†).

The favorable interfacial interaction between fillers and polymer matrices was also noted by the glass transition temperature (T_g) shift towards higher temperatures.[29,30] As shown in Fig. S7 in the ESI,† a significant shift in the T_g value from 187 to 198 °C occurs for the PSF-based MMMs. For the Pebax®1657-based MMMs, a medium increase in the T_g value from −56 to −50 °C was found. The above results suggest a strong interfacial interaction between the ZIF-7-I fillers and PSF/Pebax possibly derived from the rigidification of the polymer chains on the surface of the fillers. In contrast, the increase in the T_g value of PDMS-based MMMs was only marginal. This result was attributed to the weaker interaction between the fillers and polymer chains.

The permeation properties for O_2 and N_2 on three types of MMMs were evaluated through the constant–volume variable–pressure method[31] (Fig. S1 in the ESI†). For the MMMs derived from PDMS and ZIF-7-II nanocrystals, sharp decrease in O_2 permeability and no enhancement in O_2/N_2 selectivity were found (Fig. 4c).

As one of the most permeable materials, PDMS has O_2 permeability as high as 500 Barrer. In contrast, O_2 almost could not penetrate into the narrow-pore ZIF-7-II frameworks. Therefore, the addition of the ZIF-7-II fillers in the PDMS matrix led to the decrease in O_2 permeability. Compared with the results for the pristine PSF and Pebax®1657 membranes, the O_2/N_2 selectivity on the MMMs containing the ZIF-7-I nanocrystals was dramatically improved (Fig. 4c and Table S1 in ESI†). The permeability of N_2 on 15 wt% ZIF-7-I-Pebax MMMs was ~1.1 Barrer, which was comparable with the values reported by Li and co-workers,[33] suggesting the reasonable fabrication and measurement procedures for the as-synthesized membranes. To probe the origin of improved selectivity, the O_2 adsorption properties of the pure and composite membranes were first measured. As shown in Fig. S8a in the ESI,† ZIF-7-II-PDMS MMMs exhibit slightly improved O_2 adsorption properties

Table 1 Single and mixed-gas permeation properties measured on the pure 6FDA/BPDA-ODA film and MMMs containing ZIF-7 fillers at 35 °C[a]

	Pure gas permeability[b] (Barrer)		Ideal selectivity	Mixed-gas permeability[c] (Barrer)		Separation factor
Membranes	O_2	N_2	O_2/N_2	O_2	N_2	O_2/N_2
Pristine PI2	1.5 ± 0.1	0.15 ± 0.01	10.0 ± 0.5	1.4 ± 0.1	0.15 ± 0.01	9.3 ± 0.5
15% ZIF-7-I-PI2	2.9 ± 0.2	0.19 ± 0.01	15.2 ± 1	2.7 ± 0.2	0.18 ± 0.01	15.0 ± 1

[a] Permeation measurements were conducted by the constant–volume variable–pressure method, and the results were averaged as the final data with deviation from three membrane samples fabricated under the same condition. [b] Pure-gas permeations were performed under 2 bar. [c] Equal-molar mixed-gas permeations were performed under 4 bar.

compared to the pristine PDMS membrane. Moreover, the experimental O_2 uptake of MMMs was much closer to the theoretical prediction, suggesting no pore blockage of ZIF-7-II by the polymer chains. In contrast, the experimental O_2 uptake on the 15 wt% ZIF-7-I-polymer (PSF or Pebax®1657) MMMs was much higher than that of the pristine polymer membranes (Fig. S8b in the ESI†). In addition, the theoretically predicted O_2 uptake on 15 wt% ZIF-7-II/polymer (PSF or Pebax®1657) MMMs was much lower than that on ZIF-7-I/polymer MMMs. The above results indicate that the intrinsic O_2 permeation ability on the ZIF-7-I phase far exceeds that on the ZIF-7-II phase. This phenomenon was also consistent with the simulated results of ZIF-7-I and ZIF-7-II for O_2 adsorption (Fig. S9 in the ESI†).

Besides, the N_2 adsorption results (Fig. S10 in the ESI†) also revealed that the gas solubility in MMMs increased upon the incorporation of the ZIF-7 nanocrystals. The N_2 uptake on ZIF-7-I-based MMMs ($\sim$1.7 $cm^3\ g^{-1}$ at 1000 kPa) was similar to that on ZIF-7-II-based MMMs, implying that the ZIF-7-I and ZIF-7-II phases within the polymers possessed sub-equal solubility and permeation property for N_2. Based on the solution-diffusion mechanism in composite membranes,[34] the diffusion coefficients of both gases were calculated from the relationship between permeability and solution coefficient. As shown in Fig. S11 in the ESI,† the O_2/N_2 diffusion selectivity for ZIF-7-I-PSF MMMs shows remarkable enhancement ($\sim$178%) compared to that of the pristine polymer membrane. Therefore, the increase in the O_2/N_2 selectivity on ZIF-7-I-PSF MMMs was mainly attributed to the considerable increase in the diffusion selectivity for O_2/N_2. This result implied that the guest-free ZIF-7-I crystals possessed a high molecular sieving effect for O_2/N_2 separation. The 15 wt% ZIF-7-I-PSF MMMs showed slight decline in the O_2 diffusion coefficients compared with the pure PSF membrane. This is a common phenomenon in glassy polymer-based MMMs.[35] The rigidified polymer region near the filler may increase the tightness of the polymer chain, leading to the decrease in the gas diffusion coefficient. This always results in an increase in selectivity compared with that of the pristine dense film. As verified by the previous DSC measurements (Fig. S7 in the ESI†), the 15 wt% ZIF-7-I-PSF MMMs exhibited higher T_g values than the original polymeric membranes. Compared with the pure Pebax film, both O_2/N_2 diffusion selectivity and solubility selectivity on 15 wt% ZIF-7-I-Pebax MMMs increased by 50% and 30%, respectively (Table S2 in the ESI†). The enhancement in diffusion selectivity was attributed to the molecular sieving effect of ZIF-7-I for O_2/N_2 separation, while the increase in solubility selectivity may be attributed to the interfacial microstructure between the soft PE segments and ZIF-7-I fillers. Further experiments are still undergoing. In view of the minimal non-ideal clusters in 15 wt% ZIF-7-I-Pebax®1657 MMM, its gas-permeation results were selected to estimate the O_2 and N_2 permeabilities of the ZIF-7-I phase using the Maxwell model.[36] The O_2 permeability and the O_2/N_2 selectivity of guest-free ZIF-7-I were calculated to be approximately 60 Barrer and 120, respectively. These values were far beyond those of zeolite 4A.[37] ZIF-7-I exhibited the highest O_2/N_2 separation performance among molecular sieves reported so far.

In order to further improve the O_2/N_2 separation performance, another two polyimides with better intrinsic performances, *i.e.*, BTDA-ODA (denoted as PI1) and 6FDA/BPDA-ODA (denoted as PI2) were used as the polymer matrices. As shown in Fig. 4d and Table S3 in the ESI,† the fabricated MMMs containing 15 wt% ZIF-7-I nanocrystals exhibit a remarkable leap for O_2/N_2 separation compared with the pristine polymer membranes. The separation performances on both MMMs reached unprecedentedly high levels (see Table S4 in the ESI†) and were well above the polymer upper bound for O_2/N_2 separation, falling in the commercially attractive region.[32,38] As shown in Table 1, the O_2/N_2 separation performances of pure-component and mixed-gas permeation are very close. Furthermore, the O_2/N_2 permeability and separation factors were also independent of the feeding pressure in mixed-gas permeation (Fig. 4e). The above results were possibly observed due to the weak competitive interaction between O_2/N_2 and hybrid membrane materials.

Conclusions

This was the first experimental demonstration for hindering the phase transition of a flexible ZIF-7 framework in polymers containing rigid chains or segments. The resulting MMMs derived from the ZIF-7-I nanocrystals displayed significant improvement in O_2/N_2 selectivity, which was mainly attributed to the considerable increase in the diffusion selectivity. Combining characterization results, it was demonstrated that the guest-free ZIF-7-I crystals possessed a molecular sieving effect for O_2/N_2 separation. The separation performance on the MMMs containing polyimide and ZIF-7-I crystals falls in the commercially attractive region; they exhibited the best performances for O_2/N_2 separation among previously reported MMMs so far. The current work provides a feasible method to control the framework flexibility of MOF materials. This work also indicates that the ZIF-7-I membranes are particularly suitable for air separation.

Conflicts of interest

There are no conflicts to declare.

Acknowledgements

This work was supported by the National Natural Science Foundation of China (21622607, 21776124, 21761132009), Jiangsu Provincial NSFC (BK20171459), Zhejiang Provincial NSFC (LR18B-060002), Foundation of Jiangsu Educational Committee of China (17KJA530004), and the Priority Academic Program Development of Jiangsu Higher Education Institutions (PAPD). Y. P. also appreciates the support from the Six Talent Peaks Project and Qing-Lan Engineering Project of Jiangsu Province. Y. L. appreciates the K. C. Wong Magna Fund in Ningbo University.

Notes and references

1 D. S. Sholl and R. P. Lively, *Nature*, 2016, **532**, 435–437.
2 E. D. Bloch, L. J. Murray, W. L. Queen, S. Chavan, S. N. Maximoff, J. P. Bigi, R. Krishna, V. K. Peterson, F. Grandjean, G. J. Long, B. Smit, S. Bordiga, C. M. Brown and J. R. Long, *J. Am. Chem. Soc.*, 2011, **133**, 14814–14822.
3 W. Zhang, D. Banerjee, J. Liu, H. T. Schaef, J. V. Crum, C. A. Fernandez, R. K. Kukkadapu, Z. Nie, S. K. Nune, R. K. Motkuri, K. W. Chapman, M. H. Engelhard, J. C. Hayes, K. L. Silvers, R. Krishna, B. P. McGrail, J. Liu and P. K. Thallapally, *Adv. Mater.*, 2016, **28**, 3572–3577.
4 N. Rangnekar, N. Mittal, B. Elyassi, J. Caro and M. Tsapatsis, *Chem. Soc. Rev.*, 2015, **44**, 7128–7154.
5 K. S. Park, Z. Ni, A. P. Cote, J. Y. Choi, R. D. Huang, F. J. Uribe-Romo, H. K. Chae, M. O'Keeffe and O. M. Yaghi, *Proc. Natl. Acad. Sci. U. S. A.*, 2006, **103**, 10186–10191.
6 A. Schneemann, V. Bon, I. Schwedler, I. Senkovska, S. Kaskel and R. A. Fischer, *Chem. Soc. Rev.*, 2014, **43**, 6062–6096.
7 J. P. Zhang, H. L. Zhou, D. D. Zhou, P. Q. Liao and X. M. Chen, *Natl. Sci. Rev.*, 2018, **5**, 907–919.
8 S. K. Elsaidi, M. H. Mohamed, D. Banerjee and P. K. Thallapally, *Coord. Chem. Rev.*, 2018, **358**, 125–152.
9 J. A. Mason, J. Oktawiec, M. K. Taylor, M. R. Hudson, J. Rodriguez, J. E. Bachman, M. I. Gonzalez, A. Cervellino, A. Guagliardi, C. M. Brown, P. L. Llewellyn, N. Masciocchi and J. R. Long, *Nature*, 2015, **527**, 357–361.
10 E. J. Carrington, C. A. McAnally, A. J. Fletcher, S. P. Thompson, M. Warren and L. Brammer, *Nat. Chem.*, 2017, **9**, 882–889.
11 Q. Shi, Z. F. Chen, Z. W. Song, J. P. Li and J. X. Dong, *Angew. Chem., Int. Ed.*, 2011, **50**, 672–675.
12 C. Zhang, R. P. Lively, K. Zhang, J. R. Johnson, O. Karvan and W. J. Koros, *J. Phys. Chem. Lett.*, 2012, **3**, 2130–2134.
13 Y. C. Pan, T. Li, G. Lestari and Z. P. Lai, *J. Membr. Sci.*, 2012, **390**, 93–98.
14 L. Q. Sheng, C. Q. Wang, F. Yang, L. Xiang, X. J. Huang, J. Yu, L. X. Zhang, Y. C. Pan and Y. S. Li, *Chem. Commun.*, 2017, **53**, 7760–7763.
15 X. L. Ma, P. Kumar, N. Mittal, A. Khlyustova, P. Daoutidis, K. A. Mkhoyan and M. Tsapatsis, *Science*, 2018, **361**, 1008–1011.
16 E. Barankova, X. Tan, L. F. Villalobos, E. Litwiller and K. V. Peinemann, *Angew. Chem., Int. Ed.*, 2017, **56**, 2965–2968.
17 S. Zhou, Y. Y. Wei, L. B. Li, Y. F. Duan, Q. Q. Hou, L. L. Zhang, L. X. Ding, J. Xue, H. H. Wang and J. Caro, *Sci. Adv.*, 2018, **4**, 8.
18 P. Zhao, G. I. Lampronti, G. O. Lloyd, M. T. Wharmby, S. Facq, A. K. Cheetham and S. A. T. Redfern, *Chem. Mater.*, 2014, **26**, 1767–1769.
19 M. He, J. F. Yao, L. X. Li, K. Wang, F. Y. Chen and H. T. Wang, *ChemPlusChem*, 2013, **78**, 1222–1225.
20 L. M. Robeson, *J. Membr. Sci.*, 2008, **320**, 390–400.
21 L. Xiang, L. Q. Sheng, C. Q. Wang, L. X. Zhang, Y. C. Pan and Y. S. Li, *Adv. Mater.*, 2017, **29**, 8.
22 Y. Li and T. S. Chung, *Int. J. Hydrogen Energy*, 2010, **35**, 10560–10568.
23 S. Aguado, G. Bergeret, M. P. Titus, V. Moizan, C. Nieto-Draghi, N. Bats and D. Farrusseng, *New J. Chem.*, 2011, **35**, 546–550.
24 W. Morris, N. He, K. G. Ray, P. Klonowski, H. Furukawa, I. N. Daniels, Y. A. Houndonougbo, M. Asta, O. M. Yaghi and B. B. Laird, *J. Phys. Chem. C*, 2012, **116**, 24084–24090.
25 J. van den Bergh, C. Gucuyener, E. A. Pidko, E. J. M. Hensen, J. Gascon and F. Kapteijn, *Chem. – Eur. J.*, 2011, **17**, 8832–8840.
26 W. X. Cai, T. Lee, M. Lee, W. Cho, D. Y. Han, N. Choi, A. C. K. Yip and J. Choi, *J. Am. Chem. Soc.*, 2014, **136**, 7961–7971.
27 A. Arami-Niya, G. Birkett, Z. H. Zhu and T. E. Rufford, *J. Mater. Chem. A*, 2017, **5**, 21389–21399.
28 H. B. Park, J. Kamcev, L. M. Robeson, M. Elimelech and B. D. Freeman, *Science*, 2017, **356**, 10.
29 J. Yu, C. Q. Wang, L. Xiang, Y. Z. Xu and Y. C. Pan, *Chem. Eng. Sci.*, 2018, **179**, 1–12.
30 K. Chen, K. Xu, L. Xiang, X. Dong, Y. Han, C. Q. Wang, L. B. Sun and Y. C. Pan, *J. Membr. Sci.*, 2018, **563**, 360–370.
31 Q. L. Song, S. K. Nataraj, M. V. Roussenova, J. C. Tan, D. J. Hughes, W. Li, P. Bourgoin, M. A. Alam, A. K. Cheetham, S. A. Al-Muhtaseb and E. Sivaniah, *Energy Environ. Sci.*, 2012, **5**, 8359–8369.
32 C. M. Zimmerman, A. Singh and W. J. Koros, *J. Membr. Sci.*, 1997, **137**, 145–154.
33 T. Li, Y. C. Pan, K. V. Peinemann and Z. P. Lai, *J. Membr. Sci.*, 2013, **425**, 235–242.
34 L. Xiang, Y. C. Pan, G. F. Zeng, J. L. Jiang, J. Chen and C. Q. Wang, *J. Membr. Sci.*, 2016, **500**, 66–75.
35 T. S. Chung, L. Y. Jiang, Y. Li and S. Kulprathipanja, *Prog. Polym. Sci.*, 2007, **32**, 483–507.
36 C. Zhang, Y. Dai, J. R. Johnson, O. Karvan and W. J. Koros, *J. Membr. Sci.*, 2012, **389**, 34–42.
37 R. Mahajan and W. J. Koros, *Ind. Eng. Chem. Res.*, 2000, **39**, 2692–2696.
38 H. K. Jeong, W. Krych, H. Ramanan, S. Nair, E. Marand and M. Tsapatsis, *Chem. Mater.*, 2004, **16**, 3838–3845.

